Uncrossability constraints in mesoscopic polymer melt simulations: Non-rouse behavior of C120H242

Uncrossability constraints in mesoscopic polymer melt simulations: Non-Rouse behavior of C120H242

J. T. Padding and W. J. Briels

Citation: J. Chem. Phys. **115**, 2846 (2001); doi: 10.1063/1.1385162
View online: http://dx.doi.org/10.1063/1.1385162
View Table of Contents: http://jcp.aip.org/resource/1/JCPSA6/v115/i6
Published by the American Institute of Physics.

Uncrossability constraints in mesoscopic polymer melt simulations: Non-Rouse behavior of $C_{120}H_{242}$

J. T. Padding[a] and W. J. Briels[b]
Computational Dispersion Rheology, Department of Applied Physics, University of Twente, P. O. Box 217, 7500 AE Enschede, The Netherlands

(Received 29 March 2001; accepted 18 May 2001)

An important feature of a melt of long polymers is that the bonds of the chains cannot cross each other. This seemingly simple fact has a great impact on the long time dynamics and rheology of the material. In this paper an algorithm is described that explicitly detects and prevents bond crossings in mesoscopic simulations of polymers. The central idea is to view the bonds as slippery elastic bands which can become entangled. The method is applied to a simulation of a coarse-grained melt of $C_{120}H_{242}$, in which each chain is represented by six blobs. The long time dynamics and zero-shear rate rheology are investigated and the relative importance of uncrossability and chain stiffness is established. As a result of the uncrossability of the chains, we observe a subdiffusive exponent in the mean square displacement of the chains, a stretching of the exponential decay of the Rouse mode relaxations, an increase of relaxation times associated with large scales, and a slowing down of the relaxation of the dynamic structure factor. These results are in agreement with results from previous microscopic molecular dynamics simulations. Finally, an increased viscosity as compared to the Rouse model is observed, which is attributed to slowly decaying interchain stress components. © *2001 American Institute of Physics.* [DOI: 10.1063/1.1385162]

I. INTRODUCTION

Experimentalists and theoriticians are fascinated by the peculiar dynamics of polymer melts. Rheological experiments reveal a nontrivial molecular weight dependence of the viscosity, and the same applies to the diffusion coefficient, which can be measured by field gradient NMR or forward recoil spectrometry techniques.[1–4] Also, neutron spin echo spectroscopy measurements have revealed a broad spectrum of characteristic times which are associated with relaxations at different length scales.[5–7] The task of theoriticians is to explain these results in terms of the simplest possible models which still embody the essential features of polymers, i.e., they are long and flexible and that their covalent bonds cannot be cut or cross. The use of such simple models containing only essential features is justified by experimental observations of universal scaling behavior of (linear) polymers of different chemical structure. This suggests that rheological properties and motions of large parts of the chain may not depend on the details of the polymers except for some species-dependent ''effective'' parameters, such as friction coefficients, and structural information may only be needed on the scale of groups of monomers. Two of the best known models in this category are the Rouse model[8] and the reptation model.[9] The former is supposed to describe the dynamics of relatively low-weight linear polymers. It assumes that the surrounding chains merely constitute a stochastic background to a chain of harmonically bound beads. The latter describes the dynamics of very long chains which are forced to move anisotropically inside effective tubes formed by entanglements with surrounding chains. Still, despite the large amount of literature on these models, many problems remain unsolved. In particular, there is no general consensus of the concept of entanglement length[10] and even the necessity to invoke reptation to explain the experimental results is not without debate (see Ref. 11 for a review on this matter).

Despite their simplicity, most polymer models require computer simulations to reveal their macroscopic properties. In the successful model applied by Kremer and coworkers, groups of monomers are represented as pure repulsive Lennard–Jones spheres and the bonded spheres are connected by a finitely extensible nonlinear elastic potential (FENE).[10,12] Alternatively, the polymer may be represented as a freely-jointed chain of hard spheres,[13] or as a chain of ellipsoidal particles.[14,15] In these models, the interactions are chosen explicitly such that bond crossings will be energetically unfavorable. Thus, an essential feature of the polymer chain is incorporated automatically. The range of the repulsive forces in these models is necessarily of the order of the maximum separation of two bonded spheres, which sets a severe limit to the number of monomers which may be represented by one sphere. Actually, one would like to have this number as large as possible, and start with detailed molecular dynamics simulations of relatively short polymer chains to determine effective interactions and friction parameters of groups of monomers by averaging out uninteresting degrees of freedom. This so-called coarse-graining of polymers may be done in numerous ways.[16–18] In this paper, a rather simple coarse-graining procedure is adopted because interactions will become soft in any case, and we think that, crucial for obtaining the right rheological properties, is not so much the

[a]Electronic mail: j.t.padding@ct.utwente.nl
[b]Electronic mail: w.j.briels@tn.utwente.nl

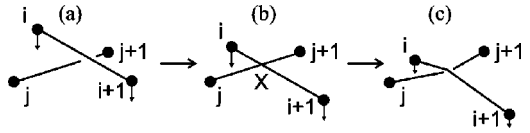

FIG. 1. The creation of an ''entanglement'': (a) Two pairs of bonded blobs are closing in on each other. (b) At a certain moment their bonds will touch. (c) An entanglement is created at the crossing point X, after which the bonds are viewed as slippery elastic bands. The elasticity will slow down the relative speed of the bonds.

interactions, but the fact that chains are not allowed to cross.[19] Therefore, we will give full attention to explicitly obeying the uncrossability constraint.

Up to now, explicit uncrossability constraints have only been implemented for Monte Carlo simulations on cubic and diamond lattices.[20–22] Simulations on lattices are however typically performed at rather low densities in order to obtain a reasonable acceptance rate of the attempted moves.[12] In order to be able to perform mesoscopic simulations at high densities, we have implemented a routine which explicitly detects and prevents bond crossings in a continuum simulation program called TWENTANGLEMENT (Twente University entanglement).[23]

One can think of many ways to implement an uncrossability constraint. Our method is based on considering the bonds as elastic bands between the bonded particles. As soon as two of these elastic bands make contact, an ''entanglement'' is created which prevents the elastic bands from crossing. This is depicted in Fig. 1. To take away any confusion: In this paper ''entanglements'' are defined as the objects which prevent the crossing of chains. Only a few of these are expected to be entanglements in the usual sense of long-lasting obstacles, slowing down the chain movement. For instance, the $C_{120}H_{242}$ chain is generally considered not to be entangled, yet many ''entanglements'' occur in the simulation. For the implementation of the algorithm, the following considerations have been taken into account: (i) The entanglement algorithm should be a simple generalization of the force routine, yet capture the essence of what an entanglement is, i.e.; (ii) an entanglement must prevent the crossing of two bonds; (iii) an entanglement should be able to dynamically slide along the backbone of the chain (i.e., not be a permanent crosslink); and (iv) an entanglement should be able to disentangle if the topology of the chain demands so.

The purpose of this paper is twofold. First, we will explain the assumptions and approximations made for the construction of the entanglement algorithm. Second, the influence of the uncrossability constraint on the dynamic behavior of relatively short coarse-grained polyethylene chains will be investigated. These results will be compared with microscopic simulations described in a previous paper,[24] with mesoscopic simulations without the uncrossability constraint, and with results from the literature.

This paper is organized as follows: In Sec. II we describe the coarse-grained simulation model and give an introduction to the entanglement constraint. Details of the entanglement constraint are given in Sec. III. This section is rather technical, so may be skipped by the reader who is interested in the results only. Section IV describes the application of the entanglement constraint to the coarse-grained melt of polyethylene $C_{120}H_{242}$. The method by which the initial box is prepared and the choice of parameters are explained. The results of the simulations are presented and discussed in Sec. V. We summarize the conclusions in Sec. VI.

II. THE SIMULATION MODEL

A. Coarse-grained interactions

Because the details of a polymer are largely unimportant for its large scale dynamics, the chain will be described in terms of groups of monomers, which we call ''blobs.'' The position $\mathbf{R}$ of each blob is defined as the center of mass position of the λ monomers which together constitute the blob:

$$\mathbf{R}=\frac{1}{M}\sum_{i=1}^{\lambda} m_i\mathbf{r}_i, \tag{1}$$

where $\mathbf{r}_i$ is the position and m_i the mass of monomer i, and M is the total mass of the blob. The complementary $3(\lambda-1)$ coordinates per blob of the microscopic system are treated as bath variables, i.e., their effects are taken into account through random forces which perturb the time evolution of the blob positions. A complete separation of time scales is assumed, such that the random force correlations decay much faster than the blob momentum correlations. In this approximation, the random force correlations may be represented by delta functions and the equations of motion are of the simplest Langevin type:[18]

$$M\frac{d^2\mathbf{R}_i}{dt^2}=-\nabla_i\chi-\zeta\frac{d\mathbf{R}_i}{dt}+\mathbf{F}_i^R. \tag{2}$$

where χ is the potential of mean force (PMF) of the blob system, and ζ is the blob friction coefficient. The friction is chosen to be independent of the blob configuration; it is related to the random force $\mathbf{F}_i^R$ through the fluctuation dissipation theorem:

$$\langle\mathbf{F}_i^R(t)\cdot\mathbf{F}_j^R(0)\rangle=6kT\zeta\delta_{ij}\delta(t), \tag{3}$$

where k is Boltzmann's constant, and T the temperature.

The potential of mean force is defined as

$$\chi(\mathbf{R}^n)=-kT\ln P_n(\mathbf{R}^n). \tag{4}$$

Here P_n is the n-blob distribution function which is determined from the microscopic system by averaging over the fast variables. The occurrence of χ in the Langevin equation ensures that the blob distributions in the coarse-grained and microscopic systems will be the same. Unfortunately, it is very hard to handle a $3n$-dimensional distribution function, so approximations need to be made. We have made the rather crude assumption that the distribution factorizes into independent nonbonded, bonded, and angular parts according to:

$$P_n(\mathbf{R}^n)=\prod_{i<j}P^{\mathrm{nb}}(R_{i,j})\prod_i P^b(R_{i,i+1})\prod_i P^{\theta}(\theta_i). \tag{5}$$

Here $\mathbf{R}_{i,j}=\mathbf{R}_i-\mathbf{R}_j$, $R_{i,j}=|\mathbf{R}_{i,j}|$, and θ_i is the angle between two consecutive bonds, $\cos\theta_i=(\mathbf{R}_{i-1,i}\cdot\mathbf{R}_{i,i+1})/$

$(|\mathbf{R}_{i-1,i}||\mathbf{R}_{i,i+1}|)$. The potential is thus approximated as a sum of nonbonded, bonded, and angular energies:

$$\chi(\mathbf{R}^n)=\sum_{i<j}\varphi^{\mathrm{nb}}(R_{i,j})+\sum_i\varphi^b(R_{i,i+1})+\sum_i\varphi^\theta(\theta_i). \tag{6}$$

The first sum is over all nonbonded pairs, the second sum over all bonded blobs, and the third sum over all groups of three consecutive blobs. Although in reality the distributions will not be completely independent, and indirect correlations between two given blobs via the surrounding blobs are important, they have been neglected here, since the focus of our work lies with the entanglements.

To determine the distribution functions, molecular dynamics simulations of polyethylene chains of 120 monomers per chain were performed at $T=450$ K, as described in Ref. 24. For the number of monomers per blob, λ, the following two considerations were taken into account: (i) λ should be large enough to allow for a significant increase of the integration timestep. For the more monomers, together, constitute a blob, the larger will be its mass and the softer will be the interactions between the blobs, and consequently, the more the timestep can be increased. However, (ii) λ should not be so large that the size of the blobs exceeds the typical diameter of the tube in the reptation picture, or in other words, the entanglement length. In that case, it would be impossible for the model to display a tube of realistic proportions. A suitable choice seemed to be $\lambda=20$ CH_2 units, which is still roughly one third of the entanglement length reported by Carella and coworkers.[25] The partial PMF's were calculated as minus kT times the logarithm of the measured distributions of blobs and fitted with simple analytical functions, as shown in Fig. 2. The nonbonded blob interaction was described by a single repulsive Gaussian pair potential:

$$\varphi^{\mathrm{nb}}(R)=c_0e^{-(R/b_0)^2}. \tag{7}$$

The bonded blob interaction was split into two parts, a repulsive term φ^{rep}, described by two Gaussians, and an attractive term φ^{att}, described by a single power law:

$$\varphi^b(R)=\varphi^{\mathrm{rep}}(R)+\varphi^{\mathrm{att}}(R), \tag{8}$$

$$\varphi^{\mathrm{rep}}(R)=c_1e^{-(R/b_1)^2}+c_2e^{-(R/b_2)^2}, \tag{9}$$

$$\varphi^{\mathrm{att}}(R)=c_3(R)^\mu. \tag{10}$$

The reason for splitting up the bonded blob interactions will become clear when we apply the uncrossability constraint. The angular potential was described as a function of the cosine of the angle:

$$\varphi^\theta(\theta)=c_4(1-\cos\theta)^\nu. \tag{11}$$

The fit parameters c_0 to c_4, b_0 to b_2, μ, and ν are listed in Table I.

B. Entanglements

An important consequence of averaging out the bath variables is that the resulting bonded and nonbonded interactions become softer and broaden their range. A comparison with $kT=3.74$ kJ/mol shows that it becomes likely that two bonds will cross. This is an unphysical process, which will make the model lose all its dynamic properties characteristic for polymer melts. For this reason, we have developed an entanglement algorithm, which explicitly detects and prevents bond crossings, and implemented it in a program called TWENTANGLEMENT.[23] The detection of crossings between bonds is achieved by means of a simple geometric argument, details of which will be given in the next section. Once an imminent bond crossing is detected, an entanglement point **X** is defined at the crossing site, as in Fig. 1(b). As the blobs continue to move, the entanglement point **X** shifts, such that it will push both bonds back to their respective sides. This is accomplished by changing the attractive potential φ^{att} between bonded blobs by replacing the blob distance $R_{i,i+1}$ by the *path length* $L_{i,i+1}$ from one blob i to the next *via* the entanglement:

$$L_{i,i+1}=|\mathbf{R}_i-\mathbf{X}|+|\mathbf{X}-\mathbf{R}_{i+1}|, \tag{12}$$

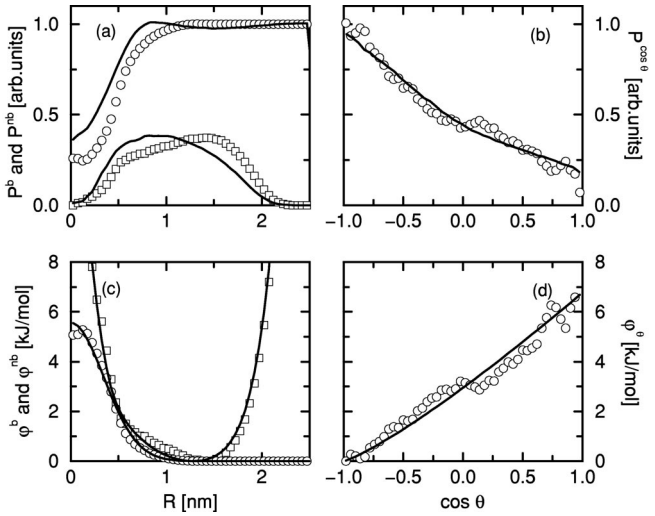

FIG. 2. Distribution functions and potentials of mean force. Using microscopic simulations, the distribution functions between nonbonded (circles) and bonded (squares) centers of mass of 20 monomer units have been determined [symbols in (a)]. Taking minus kT times the logarithm, partial potentials of mean force are obtained [corresponding symbols in (c)], which are then fitted with simple analytical functions [solid lines in (c), Eqs. (7) to (10) in the text]. In the same way, the angular potential of mean force has been determined [symbols in (b), symbols and solid line in (d), Eq. (11)]. Mesoscopic simulations with these potentials and the uncrossability constraint yield the distributions given by the solid lines in (a) and (b).

TABLE I. Parameters for the potentials of mean force, obtained from fits of the distribution functions, as explained in the text.

Parameter	Value	Units
c_0 (nonbonded)	5.557	kJ mol^{-1}
b_0	0.491	nm
c_1 (bonded)	10.47	kJ mol^{-1}
b_1	0.261	nm
c_2	3.498	kJ mol^{-1}
b_2	0.671	nm
c_3	5.3	10^{-3} kJ mol^{-1} nm$^{-\mu}$
μ	10	
c_4 (angular)	3.011	kJ mol^{-1}
ν	1.2	

$$\varphi^{\mathrm{att}}(L_{i,i+1}) = c_3 (L_{i,i+1})^{\mu}. \tag{13}$$

The entanglement position $\mathbf{X}$ is fixed by requiring that the total attractive potential energy of the entangled bonds $\varphi^{\mathrm{att}}(L_{i,i+1}) + \varphi^{\mathrm{att}}(L_{j,j+1})$ is at its minimum. This is equivalent to requiring equilibrium of forces at the entanglement. In a sense, the original bonds are replaced by slippery elastic bands which go via the entanglements. The finite extensibility of the bands prevents entangled chains from crossing each other. The expression for the path length that is given here is only valid in case of just one entanglement between two pairs of bonded blobs. The algorithm allows for any number of entanglements between pairs of bonded blobs. To this end, the path length concept has been trivially modified. A detailed description of this and other aspects of the entanglement algorithm will be given in the next section.

The replacement of blob distances by path lengths in the bonded part of the potential energy, of course, changes the structural properties of the model. As shown in Fig. 2, however, the mesoscopic distribution functions obtained by this method are hardly different from the ones obtained from the microscopic simulation.

III. DETAILED DESCRIPTION OF THE ENTANGLEMENT ALGORITHM

A. Overview

The entanglement algorithm described below can be placed in the force routine of any standard molecular or stochastic dynamics program. A typical update in such a program consists of evaluating the forces that act on the particles, using these to calculate the accelerations of the particles and subsequently updating the particle velocities and positions. The entanglement algorithm in the force routine consists of the following three parts: (1) Given the new blob positions and the order of blobs and entanglements in the chains, move the entanglements to their new positions and calculate the forces that act on the blobs. (2) Detect new entanglements and disentanglements caused by the movements of the blobs and the entanglements. (3) If possible, let entanglements slip across blobs or each other (nontrivial moves). The details of each of these parts will be described in the following subsections.

B. Moving entanglements

Suppose entanglements already exist. In the mesoscopic model, the entanglements have no volume and are fully characterized by their positions $\mathbf{X}_k$. As was already mentioned in the previous section, the attractive potential φ^{att} is redefined to be a function of the path length $L_{i,i+1}$. In case the bond runs from blob i, via p consecutive entanglements, to blob $i+1$ (see Fig. 3), the path length is defined as:

$$L_{i,i+1} = |\mathbf{R}_i - \mathbf{X}_1| + |\mathbf{X}_1 - \mathbf{X}_2| + \ldots + |\mathbf{X}_p - \mathbf{R}_{i+1}|. \tag{14}$$

Since each blob represents a large collection of monomer units, the heavy backbone of the mesoscopic chain will, in general, move very sluggishly. This is in contrast to an entanglement, which at the atomic level includes only a few monomer units. Consequently, the timescale with which the entanglement position adjusts itself is much shorter than the timescale with which the polymer backbone is moving. Effectively, on the coarse-grained time scale, there will be an equilibrium of forces at the entanglements. Such an equilibrium of forces in a system with n blobs and p entanglements is achieved by the following minimization:

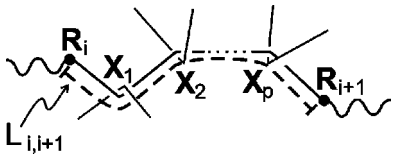

FIG. 3. Definition of the path length $L_{i,i+1}$ between bonded blobs at $\mathbf{R}_i$ and $\mathbf{R}_{i+1}$, Eq. (14).

$$\Phi^{\mathrm{att}}(\mathbf{R}^n) = \min_{\mathbf{X}^p} \sum_i \varphi^{\mathrm{att}}[(L_{i,i+1}(\mathbf{R}^n, \mathbf{X}^p)], \tag{15}$$

i.e., the entanglement positions are determined by the requirement that the total attractive energy be at its minimum (the blobs are kept at their respective positions). This minimum energy is the contribution Φ^{att} of the attractive part to the total potential energy Φ of the system. The other contributions, Eqs. (7), (9), and (11), are calculated in the usual way from the blob positions, and together constitute the remainder Φ^r of the potential energy, i.e., $\Phi = \Phi^{\mathrm{att}} + \Phi^r$. At each timestep, the dynamics program will need the forces on the blobs in order to update their velocities and positions. The minimization in Eq. (15) does not complicate the evaluation of the force on a blob i since $(\partial \Phi^{\mathrm{att}} / \partial \mathbf{X}_k) = 0$ at the minimum:

$$\mathbf{F}_i = -\frac{\partial \Phi^{\mathrm{att}}}{\partial \mathbf{R}_i} - \sum_k \left(\frac{\partial \Phi^{\mathrm{att}}}{\partial \mathbf{X}_k} \right) \cdot \left(\frac{\partial \mathbf{X}_k}{\partial \mathbf{R}_i} \right) - \frac{\partial \Phi^r}{\partial \mathbf{R}_i}$$

$$= -\frac{\partial}{\partial \mathbf{R}_i} (\Phi^{\mathrm{att}} + \Phi^r). \tag{16}$$

From the definition of the path length, Eq. (14), it is clear that the attractive force $\mathbf{f}_i^{\mathrm{att}}$ on blob i due to the elastic band between blobs i and $i+1$ is always directed along $\mathbf{R}_i - \mathbf{X}_1$:

$$\mathbf{f}_i^{\mathrm{att}} = -\frac{\partial \varphi^{\mathrm{att}}(L_{i,i+1})}{\partial \mathbf{R}_i} = -\frac{\partial \varphi^{\mathrm{att}}(L_{i,i+1})}{\partial L_{i,i+1}} \frac{\partial L_{i,i+1}}{\partial \mathbf{R}_i}$$

$$= -c_3 \mu (L_{i,i+1})^{\mu - 1} \frac{\mathbf{R}_i - \mathbf{X}_1}{|\mathbf{R}_i - \mathbf{X}_1|}, \tag{17}$$

and, correspondingly, the force due to this elastic band on blob $i+1$ is always directed along $\mathbf{R}_{i+1} - \mathbf{X}_p$, see Fig. 3.

It is important to stress that we have constructed a system in which the total energy is conserved. No work is done on the entanglements because the net force is always zero. Also, the entanglements bear no mass and hence have no kinetic energy. However, the Hamiltonian is history dependent. To calculate the forces at time t, we need information about the number of entanglements and their positions along the backbones of the chains, which is a result of events at times $t' < t$. In this respect the ensemble is not canonical.

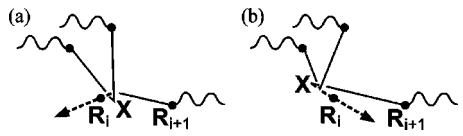

FIG. 4. The gradient of the attractive energy has a singularity at $\mathbf{R}_i$. Near this point the magnitude of the attractive force on the entanglement $\mathbf{X}$ stays approximately constant, while its direction is given by the unit vector from $\mathbf{X}$ to $\mathbf{R}_i$ [cf. Eq. (17)]. This direction changes promptly near $\mathbf{R}_i$ (dashed arrow).

The reader may wonder why the repulsive term of the bonded blob interaction, Eq. (9), was not redefined to be a function of the path length, as was realized for the attractive term. The main reason is that the equilibrium position of the entanglement would not be uniquely defined if lower repulsive energies were associated with increased path lengths. Local minima would emerge in which the minimization procedure could be trapped. Moreover, direct repulsion between the centers of bonded blobs is needed to keep the angular forces from growing too large. A potential defined in terms of angle θ, such as Eq. (11), results in a torque between two bonds. If either one of the bond lengths tends to zero, the force on the blob will go infinite, which is highly undesirable.

We end this subsection by mentioning a subtlety involved in the minimization of the attractive energy. Most effective minimization procedures require evaluations of both functions and gradients, i.e., forces. The total force on an entanglement is the sum of the forces along its four arms. Each of these forces is minus the force on its neighbor along the relevant arm. Now, for example, while moving $\mathbf{X}$ in Fig. 4 at constant blob positions $\mathbf{R}$, the force on $\mathbf{X}$ has a singularity at $\mathbf{R}_i$, as elucidated in the figure. Notice that the order of objects is not changed in this step of the entanglement algorithm; only in the last step will we check for a possible slip across the blob. Now the above singularity will cause the minimization to converge erroneously if at all. We remedy this problem by adding, at short distances between $\mathbf{X}$ and $\mathbf{R}_i$, an extra repulsive force

$$\mathbf{g}^{\mathrm{add}} = -c_3\mu(L_{i,i+1})^{\mu-1}\left(1-\frac{r}{\delta}\right)\frac{\mathbf{R}_i-\mathbf{X}}{|\mathbf{R}_i-\mathbf{X}|} \quad (r<\delta) \tag{18}$$

$$r = |\mathbf{R}_i-\mathbf{X}|, \tag{19}$$

on the entanglement, and a corresponding force $\mathbf{f}_i^{\mathrm{add}} = -\mathbf{g}^{\mathrm{add}}$ on blob i. At short distances this extra repulsive force on the entanglement counteracts the attractive force $\mathbf{g}^{\mathrm{att}} = -\mathbf{f}_i^{\mathrm{att}}$, and prevents the distance r from becoming too small. Of course, in the next step it must be checked if it is profitable to interchange the order of $\mathbf{X}$ and $\mathbf{R}_i$. A similar procedure must be applied to all pairs of connected objects coming close to each other. The value of δ was chosen equal to 10^{-4} nm, small enough to have a negligible impact on the configurations of the entangled chains, but allowing for a successful convergence of the minimization procedure.

C. Detecting new (dis)entanglements

In contrast to crosslinks in rubbers, entanglements have a finite lifetime and are continuously appearing and disappearing. In the model that is developed here, a polymer chain is viewed as a succession of objects, be they blobs or entanglements, connected by line segments. During the simulation, we keep track of all unattached pairs of line segments which are close together. They may, for instance, be extracted from the blob neighbor list. For each pair of line segments, and at each instant of time, the following triple product is calculated:

$$V_{ij} = (\mathbf{r}_i-\mathbf{r}_j)\cdot((\mathbf{r}_{i+1}-\mathbf{r}_i)\times(\mathbf{r}_{j+1}-\mathbf{r}_j)), \tag{20}$$

in which i and $i+1$ label two consecutive objects along a chain, i.e., define the first line segment. The second line segment is defined by j and $j+1$ [see Fig. 1(a)]. Note that the absolute value of the triple product is the volume of the parallelepiped defined by the vectors $\mathbf{r}_{i+1}-\mathbf{r}_i$, $\mathbf{r}_{j+1}-\mathbf{r}_j$, and $\mathbf{r}_i-\mathbf{r}_j$. There are two possibilities for the ''volume'' V_{ij} to become zero.[26] First, if the distance between the two line segments becomes zero, and, second, if the two line segments are parallel. In a molecular or stochastic dynamics simulation, the latter possibility can be neglected (the chance of two lines running *exactly* parallel at any time is extremely small, even considering the limited machine precision), so if V_{ij} changes sign from one time to the next, a possible bond crossing has occurred.[27] However, Eq. (20) does not distinguish between the physical crossing of two finite line segments and the crossing of two infinite lines. An additional check has to be made to be sure that the crossing is taking place along the physical part of the two finite line segments. In order to calculate the exact crossing point, first the exact time of crossing during the last time step must be calculated. Although in principle this involves solving a third order equation, it is found empirically that solving a linear interpolation of V_{ij} in time gives nearly the same time of crossing. Having determined the positions of the objects at this time, the next task is to find the position $\mathbf{X}$, where the two line segments have crossed [see Fig. 1(b)]. To this end define the parameters λ_1 and λ_2 by

$$\mathbf{X} = \mathbf{r}_i+\lambda_1(\mathbf{r}_{i+1}-\mathbf{r}_i) = \mathbf{r}_j+\lambda_2(\mathbf{r}_{j+1}-\mathbf{r}_j), \tag{21}$$

i.e., λ_1 defines the crossing point on the line through objects i and $i+1$, with $\lambda_1=0$ at object i and $\lambda_1=1$ at object $i+1$, and correspondingly for λ_2. These are three equations with two unknowns, λ_1 and λ_2, so any one equation can be dropped and the remaining two be solved (this stems with the fact that the line segments are already confined to a plane in 3-D space). A physical crossing between the two line segments has occurred if the crossing point lies between both i and $i+1$ and j and $j+1$, i.e.,

$$(0<\lambda_1<1)\wedge(0<\lambda_2<1). \tag{22}$$

The algorithm now proceeds as follows: An entanglement is created, initially at the position $\mathbf{X}$, where the two line segments have crossed each other. In the next timestep, the minimization of the attractive energy will move the new en-

tanglement to its equilibrium position, and the entanglement will contribute to the elastic forces between chains [Fig. 1(c)].

We would like to point out the fact that, in the developed model, two attached (consecutive) line segments can never entangle because the four objects which are connected by an entanglement will all have to be different. If either two objects are the same, the volume V_{ij} between the line segments is always zero and never changes sign.

After an entanglement is created, the associated volume V_{ij} will serve to detect future disentanglements. If the volume V_{ij} of the four objects surrounding an entanglement changes sign from one time to the next, a possible disentanglement has occurred. Additional checks are made in exactly the same way as described for the creation of entanglements, i.e., Fig. 1 may also be read backwards.

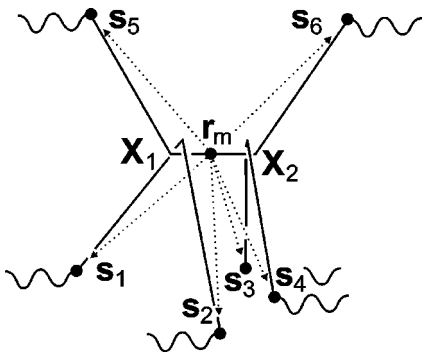

FIG. 5. Two entanglements at $\mathbf{X}_1$ and $\mathbf{X}_2$ are allowed to slip past each other if the two arms of the first entanglement ($\mathbf{s}_1$ and $\mathbf{s}_2$) can both pass over the two arms of the second entanglement ($\mathbf{s}_3$ and $\mathbf{s}_4$). The reverse case is also possible.

D. Non-trivial moves

While searching for its equilibrium position, an entanglement can move freely along the chain between two adjacent objects. At a certain moment, however, the attractive energy would be lower if the entanglement could slip past a blob one position further along the chain backbone, or to the other side of the next entanglement, or, in other words, if the order of objects within a chain would be altered. The order-altering moves are not trivial, but important for a realistic treatment of the entanglement constraints. The algorithm detects if an entanglement has a natural tendency to get close to either one of its adjacent objects by measuring the distance to these objects. If the distance becomes smaller than a prescribed value ε, i.e.,

$$|\mathbf{r}_i - \mathbf{X}| < \varepsilon, \tag{23}$$

where $\mathbf{r}_i$ is the position of the adjacent object and ε is sufficiently small compared to the average bond length, a subalgorithm will check order-altering moves. The value of ε was chosen equal to 10^{-2} nm, much smaller than the average bond length of roughly 1.5 nm. The subalgorithm makes the following checks:

1. If the object which is approached is another entanglement go to 2; if it is a blob go to 3.
2. Check if it is physically possible for one entanglement to slip past the other. If it is possible, swap the order in which the entanglements appear in the chain backbone. Otherwise do not swap. Back to main program.
3. If the blob lies at the extremum of a chain, remove the entanglement and go back to the main program. Otherwise go to 4.
4. If a slip past the blob results in an entanglement of a line segment with itself, remove the entanglement (*vide infra*) and go back to the main program. Otherwise go to 5.
5. If a slip past the blob results in disentanglement, remove the entanglement. Otherwise slip the entanglement past the blob. Back to main program.

If the entanglement has survived the slip past the adjacent object, the algorithm will find a new equilibrium position in the next timestep. Only one slip per timestep is allowed for each entanglement. In the following, we will clarify the various checks which are made in the subalgorithm.

Suppose two entanglements are very close to each other, as in Fig. 5. The mean position of the two entanglements, $\mathbf{r}_m$, will then be very close to both entanglement positions, $\mathbf{X}_1$ and $\mathbf{X}_2$. Define $\mathbf{s}_1$ to $\mathbf{s}_6$ as the vectors going from $\mathbf{r}_m$ to the surrounding six objects with positions $\mathbf{r}_1$ to $\mathbf{r}_6$, in formula:

$$\mathbf{r}_m = \tfrac{1}{2}(\mathbf{X}_1 + \mathbf{X}_2), \tag{24}$$

$$\mathbf{s}_i = \mathbf{r}_i - \mathbf{r}_m . \tag{25}$$

Now it is assumed that the two entanglements can swap if the two arms connected to the first entanglement, $\mathbf{s}_1$ and $\mathbf{s}_2$, *both* go over the two arms connected to the second entanglement, $\mathbf{s}_3$ and $\mathbf{s}_4$, or the other way around. In the first case, we demand that the projections of $\mathbf{s}_3$ and $\mathbf{s}_4$ onto the plane defined by $\mathbf{s}_1$ and $\mathbf{s}_2$ both fall in between $\mathbf{s}_1$ and $\mathbf{s}_2$. To make this mathematically explicit: Both $\mathbf{s}_3$ and $\mathbf{s}_4$ must lie in

$$\mathcal{R} = \{\mathbf{r} \in \mathbb{R}^3 | \mathbf{r} = l_1\mathbf{s}_1 + l_2\mathbf{s}_2 + l_3(\mathbf{s}_1 \times \mathbf{s}_2), \\ l_1 \in \mathbb{R}^+, l_2 \in \mathbb{R}^+, l_3 \in \mathbb{R}\}, \tag{26}$$

i.e., any vector $\mathbf{r}$ in $\mathcal{R}$ must have positive components along $\mathbf{s}_1$ and $\mathbf{s}_2$ in the basis $\{\mathbf{s}_1, \mathbf{s}_2, \mathbf{s}_1 \times \mathbf{s}_2\}$. For a given vector $\mathbf{r}$ these components are

$$l_1(\mathbf{r}) = \frac{(\mathbf{r}\cdot\mathbf{s}_1)s_2^2 - (\mathbf{r}\cdot\mathbf{s}_2)(\mathbf{s}_1\cdot\mathbf{s}_2)}{s_1^2 s_2^2 - (\mathbf{s}_1\cdot\mathbf{s}_2)^2}, \tag{27}$$

$$l_2(\mathbf{r}) = \frac{(\mathbf{r}\cdot\mathbf{s}_2)s_1^2 - (\mathbf{r}\cdot\mathbf{s}_1)(\mathbf{s}_1\cdot\mathbf{s}_2)}{s_1^2 s_2^2 - (\mathbf{s}_1\cdot\mathbf{s}_2)^2}. \tag{28}$$

If all four numbers $l_1(\mathbf{s}_3)$, $l_2(\mathbf{s}_3)$, $l_1(\mathbf{s}_4)$, and $l_2(\mathbf{s}_4)$ are positive, the entanglements can swap. Now $\mathbf{s}_1 \cdot \mathbf{s}_2 = s_1 s_2 \cos\varphi$, with φ the angle between the two arms $\mathbf{s}_1$ and $\mathbf{s}_2$. Since these are never exactly parallel, the denominators in Eqs. (27) and (28) are always positive, so only the nominators need to be calculated. As already mentioned, the inverse is also possible: The entanglements can swap if the projections of $\mathbf{s}_1$ and $\mathbf{s}_2$ onto the plane defined by $\mathbf{s}_3$ and $\mathbf{s}_4$ both fall in between $\mathbf{s}_3$ and $\mathbf{s}_4$.

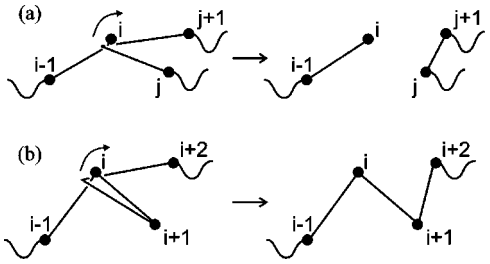

FIG. 6. (a) A slip past the last blob of a chain results in disentanglement. (b) If a chain is entangled with itself and the loop is shrinking as far as to pass through only one object apart from the entanglement, a selfdisentanglement will occur.

Now suppose the entanglement is near a blob. The subalgorithm checks if this blob is the first or last blob of the chain, because then a slip past this blob means that it is slipping off the end of the chain [Fig. 6(a)]. Usually this is not the case and the program checks if a slip past the blob results in an entanglement of two consecutive line segments, as indicated in Fig. 6(b). This happens if a chain is entangled with itself, and the loop shrinks as far as to pass through only one object apart from the entanglement. Since all four arms of an entanglement have to end at different objects, the entanglement will simply be released in this case. This is called a self-disentanglement.

Finally, it is checked if a slip past a blob results in a disentanglement. Suppose two (parts of) chains are entangled. One (part of the) chain is going from an object at $\mathbf{r}_1$, via the entanglement at $\mathbf{X}$, to an object at $\mathbf{r}_2$, and the other (part of the) chain is going from $\mathbf{r}_3$, via the entanglement, to $\mathbf{r}_4$, as in Fig. 7. Due to the very definition of an entanglement, it will always be positioned inside the tetrahedron formed by $\mathbf{r}_1$, $\mathbf{r}_2$, $\mathbf{r}_3$, and $\mathbf{r}_4$. Although in principle, entanglements may occur in one of many complicated forms, the simplest situation shown in Fig. 8(a) is by far the most probable, and we will assume that we will always have to deal with this simple unwinded form. Now suppose the entanglement wants to slip past a blob at $\mathbf{r}_4$. It will depend on the orientation of the line segment between the blob at $\mathbf{r}_4$ and the next object at $\mathbf{r}_5$ whether the entanglement will continue to exist, or must be abolished. Given the unwinded form of the entanglement, it must be abolished if the line segment $\mathbf{r}_5-\mathbf{r}_4$, or its continuation, passes through the $\mathbf{r}_1-\mathbf{r}_2-\mathbf{r}_3$ face of the tetrahedron, as in Fig. 7(b). In all other cases, as in Fig. 7(a), a new entanglement equilibrium position must be searched at the other side. A mathematical criterion is easily

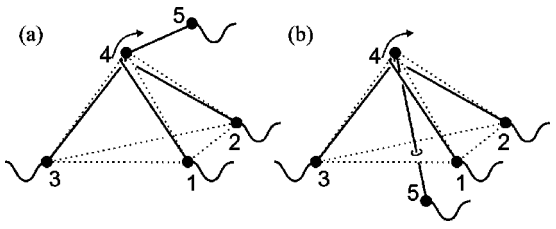

FIG. 7. (a) The entanglement X slips past blob 4 if the (extension of the) line from blob 4 to object 5 does not cross the 1-2-3 face of the tetrahedron (dotted lines). (b) The chain disentangles if this face is crossed.

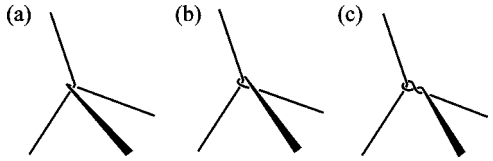

FIG. 8. The uncrossability constraint does not distinguish between different link windings. Windings (a), (b), and (c) are all equivalent to the algorithm. Obviously types (b) and (c) will be highly improbable.

obtained by equating the expression for a point in the $\mathbf{r}_1-\mathbf{r}_2-\mathbf{r}_3$ face of the tetrahedron with the expression for a point along the $\mathbf{r}_5-\mathbf{r}_4$ line,

$$\mathbf{r}_3+l_1(\mathbf{r}_1-\mathbf{r}_3)+l_2(\mathbf{r}_2-\mathbf{r}_3)=\mathbf{r}_4+l_3(\mathbf{r}_5-\mathbf{r}_4), \tag{29}$$

which can be solved for the parameters l_1, l_2, and l_3. A disentanglement will occur only if

$$(l_1>0)\wedge(l_2>0)\wedge(l_1+l_2<1)\wedge(l_3>0). \tag{30}$$

This completes the description of the nontrivial moves.

E. Increasing the speed of the algorithm

The introduction of the entanglement algorithm in a standard molecular or stochastic dynamics program will cause a lot of computational overhead. The calculations concerning nontrivial moves are quite complicated, but they do not occur very often and do not consume a considerable part of the cpu time. For the detection of new entanglements, in principle, all line segment pairs must be checked. Much time is saved by looping over the standard list of close neighbors and considering the line segments attached to these particles. The computational costs are then comparable to the costs of evaluating nonbonded forces in a standard program. The slowest part of the entanglement algorithm is the equilibration step where, in principle, the total attractive energy, Eq. (15), has to be minimized. However, the minimization can be split up in several independent parts by recognizing the fact that moving an entanglement on one side of a blob will not influence the attractive energy residing in the bonds which are connected to an entanglement on the other side of the blob (unless there is a path *around* the blob leading to the other entanglement without encountering any other blobs). For instance, in Fig. 9, the parts indicated by "1" and "2" can be equilibrated independently. Despite this fact, the minimization can still consume between 70 and 95 percent of the total time spent in the entanglement algorithm, depending on the efficiency of the minimization procedure and the desired accuracy. In this work, we demanded a relative energy con-

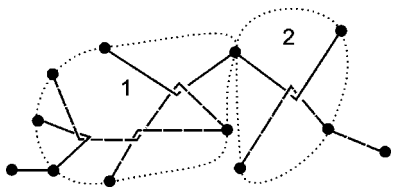

FIG. 9. The minimization to determine the positions of the entanglements between these four chains can be split up in two independent parts, indicated by the dotted lines.

vergence of 10^{-8}. A stochastic dynamics program using the entanglement algorithm was roughly 10 times slower than the same program without entanglement constraints. The advantage of being able to coarse-grain, however, has more than compensated this unfavorable factor. More importantly, it is now possible to investigate the influence of the uncrossability constraint on all kinds of dynamic properties by comparing results with and without use of the entanglement algorithm.

IV. SYSTEM PREPARATION

A. Introduction

In Sec. II, we described a possible coarse-graining procedure to arrive at a mesoscopic melt of chains, each represented by $N=6$ blobs, starting from a microscopic simulation of a $C_{120}H_{242}$ melt. In the remaining part of this paper, the influence of the uncrossability constraint on the dynamics and rheology of this system will be made explicit by comparing results of entangled and unentangled simulations. To discern effects of chain stiffness, some additional simulations will be described in which the angular potential was set to zero. In this section, we will describe how the initial boxes were created and how the friction coefficient was determined.

B. Preparation of the initial boxes

For a correct sampling of the pressure tensor autocorrelation, it is very important that the initial configuration with which the simulation will be started has no average stress. This puts forward many difficulties for molecular dynamics simulations of microscopic chains. However, unlike microscopic chains, relaxed initial configurations of mesoscopic chains are realized with comparative ease due to the softness of the interactions. Initial configurations of the chains were generated according to the distribution functions obtained from the microscopic simulations (see Fig. 2). A total of 120 chains were placed and oriented randomly in each simulation box, at a density $\rho=0.761$ g/cm^3, which is equal to the microscopic density. The nonbonded interaction parameter (c_0) was set to 1/10th of its final value in order to gently push blobs with large overlap apart, while allowing all bonds to cross each other. After this initial homogenization, the nonbonded interaction parameter was gradually increased to reach its final value. After equilibration, the initial boxes for the unentangled simulations were ready. An initial box for an entangled simulation was produced by switching on the uncrossability constraint and letting the entanglements form. The total number of entanglements was monitored and observed to reach an equilibrium value (in an average sense) within a few nanoseconds. Because entanglements are continuously created and annihilated, the number of entanglements was observed to fluctuate around an average value of 560 with a standard deviation of 40. In a future article, details will be given of entanglement distributions and time correlation functions.

C. Determination of the friction coefficient

The Langevin equation of motion, Eq. (2), contains one parameter, the blob friction coefficient ζ, that has not yet been fixed. It must be emphasized that, apart from the lengths δ and ε in the entanglement algorithm, which must be chosen small enough, the friction coefficient is the only free parameter of our model. The Langevin stochastic dynamics method has been used to perform simulations of polymer chains by several other authors among whom are Kremer and Grest.[12] These authors effectively established a coupling between the system and a heat bath in order to keep the system at some desired temperature. In order not to influence the chain dynamics too much, they had to choose the friction coefficient much smaller than the effective friction between the beads of the polymers, which is caused by the mutual interactions and relative motions of the beads and which determines dynamic properties, such as diffusion. In this paper, however, the system has been coarse-grained to a much higher level and the interactions have become very soft. As a consequence, besides acting as a thermostat, the friction coefficient ζ has acquired the meaning of a *physical* friction. One might ask, therefore, if the friction model that is applied here (isotropic, delta-correlated friction) is not too much of a simplification. Indeed, somewhat more complicated friction models have been used in the literature, i.e., in DPD methods, but these models do not do justice to all details of the movements on the coarse-grained level. Obviously, finding the right friction model will be a tremendous task (see, for instance, Ref. 18 in which much effort is taken to correctly describe the frictional interactions in a dumbbell of blobs). However, the purpose of this paper is not to find the best possible friction model, yet to test the entanglement algorithm. It will be shown that the simple approach combined with the entanglement algorithm yields results which already deviate substantially from the Rouse case.

In this work, the blob friction coefficient was chosen such that the chains' center of mass diffusion coefficient D of the entangled mesoscopic system matched the one measured in the microscopic $C_{120}H_{242}$ system. Notice that this is the bare friction coefficient, which goes into the Langevin equation and is not necessarily related to the chains' diffusion coefficient D by $\zeta=kT/(ND)$ with $N=6$ like it would have been for a melt of Rouse chains. In fact from a number of test calculations we deduced that the friction "frequency" $\xi=\zeta/M$, which for a Rouse chain would be independent of the number of monomers used to define a blob, must be chosen equal to 8.0 ps^{-1}, while in a previous study[24] we found that the Rouse friction frequency of a $C_{120}H_{242}$ chain at 450 K equals 19.0 ps^{-1}. Apparently, the entanglements introduced a substantial extra friction to the chains.

The Langevin equation was integrated using the algorithm of Allen[28] (or, equivalently, Van Gunsteren and Berendsen[29]). Given the choice of the friction, a time step $\Delta t=0.1$ ps was found to be small enough to accurately integrate the equations of motions. The simulations were run up to 4×10^6 timesteps corresponding to 0.4 microseconds.

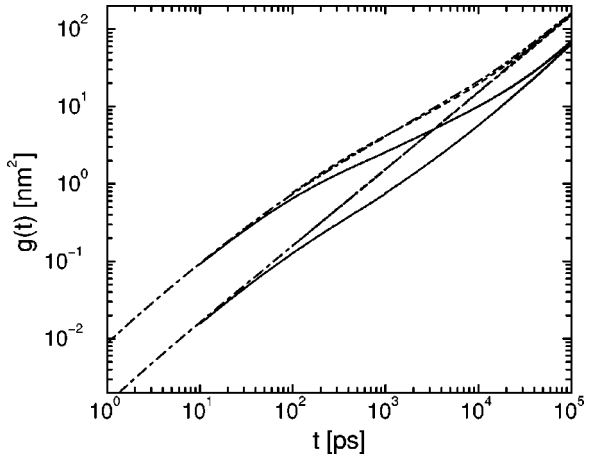

FIG. 10. Mean square displacements of entangled chains (solid), and unentangled chains with (dot-dashed) or without (dashed) chain stiffness. The upper curves are the mean square displacements of the blobs, Eq. (31), the lower curves of the center of mass of the chain, Eq. (32).

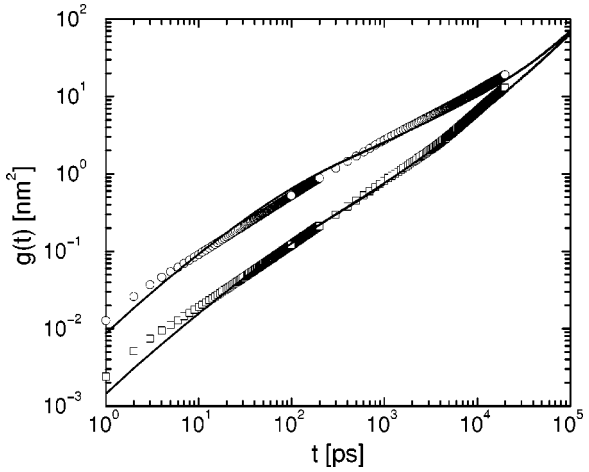

FIG. 11. Mean square displacements of entangled mesoscopic chains (solid lines) compared with the results of microscopic molecular dynamics simulations.[24] Blob mean square displacements are indicated by circles, chain center of mass mean square displacements by squares.

V. RESULTS

A. Mean square displacement

Two time-dependent mean square displacements $g_{\mathrm{bl}}(t)$ and $g_{\mathrm{cm}}(t)$ have been measured and are shown in Fig. 10. They are defined as follows:

$$g_{\mathrm{bl}}(t)=\frac{1}{N}\sum_{i=1}^{N}\langle[\mathbf{R}_i(t)-\mathbf{R}_i(0)]^2\rangle, \tag{31}$$

$$g_{\mathrm{cm}}(t)=\langle[\mathbf{R}^{\mathrm{cm}}(t)-\mathbf{R}^{\mathrm{cm}}(0)]^2\rangle, \tag{32}$$

where $\mathbf{R}_i$ is the position of the ith blob and $\mathbf{R}^{\mathrm{cm}}$ is the center of mass position of the chain of length N. The chains' center of mass mean square displacements of the unentangled chains (dashed and dot-dashed lines) are almost perfectly linear with time for all times, as is the case for Rouse chains. Also, the blob mean square displacement of the unentangled chain without angular potential can perfectly be described by the Rouse model (not shown). Adding an angular potential produces only small deviations from the Rouse model, caused by faster relaxations at smaller scales. This will become apparent in the next subsection when the Rouse modes are analyzed. In the entangled case (solid lines), both the blob and center of mass mean square displacements are slowed down considerably after 100 ps.

In Fig. 11, the results of microscopic molecular dynamics simulations (symbols) are compared with the entangled mesoscopic results (solid lines). In both cases a sublinear exponent (t^x, with $x<1$) in the center of mass mean square displacement is observed. A similar subdiffusive exponent is observed in both simulation[30] and neutron spin echo spectroscopy[5] results of a $C_{100}H_{202}$ melt. Good quantitative agreement of the minimim exponent is obtained for $g_{\mathrm{cm}}(t)$: $x=0.80$ and $x=0.77$ for the microscopic and mesoscopic models respectively and $x=0.83$ for a $C_{100}H_{202}$ chain from literature.[5] The influence of the entanglement algorithm on $g_{\mathrm{bl}}(t)$ seems to be slightly too strong: $x=0.65$ (microscopic) and $x=0.56$ (mesoscopic). In view of the crudeness of the coarse-grained interaction model, we find this acceptable.

The success of the entanglements and the unimportance of the angular dependent part of the potential in describing the subdiffusive regimes make it highly improbable that these regimes should results from internal, single chain properties.

For long times, the center of mass diffuses freely. From this regime we can determine the self-diffusion coefficient according to

$$D=\lim_{t\to\infty}\frac{g_{\mathrm{cm}}(t)}{6t}. \tag{33}$$

Pearson *et al.* have measured self-diffusion coefficients by means of field gradient NMR at 450 K experimentally for a large range of molecular weights, although not for the weight of $C_{120}H_{242}$ chains.[1] An interpolation of their data yields $D_{\mathrm{exp}}\approx 0.67\times10^{-6}\mathrm{cm}^2/\mathrm{s}$. The microscopic simulation yielded $D=1.09\times10^{-6}$ cm^2/s, overestimating the experimental result a bit. Even though the friction ξ was determined by matching the diffusion coefficient of the entangled mesoscopic model with that of the microscopic model, this matching was not perfect, and a slightly different result was obtained: $D=0.93\times10^{-6}$ cm^2/s. Without the uncrossability constraint, much larger diffusion coefficients were measured: $D=2.56\times10^{-6}$ cm^2/s with, and $D=2.52\times10^{-6}$ cm^2/s without angular potential. This is close to the Rouse model predicted diffusion coefficient of $D=2.78\times10^{-6}$ cm^2/s, using $T=450$ K, $N=6$, and $\xi=8$ ps^{-1}.

Of course, the friction coefficients of the unentangled systems might have been varied as well to match the microscopic diffusion coefficient, but then the results would not have agreed with those of the microscopic simulations at shorter time scales. It is the merit of our entangled model that it describes the motions of the chains and parts of them both on the intermediate and on the long time scales. This statement will be substantiated in the following subsections.

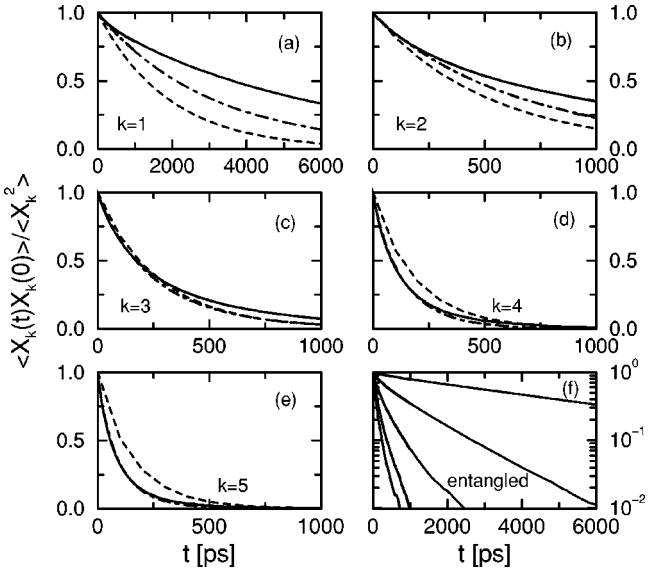

FIG. 12. Rouse mode autocorrelation functions of entangled chains (solid), and unentangled chains with (dot-dashed) or without (dashed) chain stiffness, for mode numbers 1 (a) to 5 (e). The results of the entangled chains are plotted on a semilogarithmic scale in (f), demonstrating nonexponential relaxation.

B. Rouse coordinates

It has been shown both experimentally[5] and by computer simulation[24] that in some time regimes, melts of intermediately long chains can be well described by the simple Rouse model. It is therefore interesting to investigate the systems in terms of Rouse coordinates:[31]

$$\mathbf{X}_k(t)=\frac{1}{N}\sum_{i=1}^{N}\mathbf{R}_i(t)\cos\left[\frac{k\pi}{N}\left(i-\frac{1}{2}\right)\right] \quad (k=0,\ldots,N-1) \tag{34}$$

Notice that in this subsection, $\mathbf{X}_k$ is the normal mode instead of an entanglement position. The motion of the center of mass is given by the zeroth mode, $k=0$. All other modes are associated with internal motions of the chain, mode k roughly corresponding with motion of a subchain of size N/k. Within the Rouse model, each of these modes relaxes independently and exponentially with a relaxation time τ_k,

$$\langle \mathbf{X}_k(t)\cdot\mathbf{X}_k(0)\rangle/\langle \mathbf{X}_k^2\rangle=\exp(-t/\tau_k), \tag{35}$$

$$\tau_k^{-1}=4W\sin^2\left(\frac{k\pi}{2N}\right), \tag{36}$$

where the relaxation rate W is a characteristic frequency of the Rouse model and is given by:

$$W=\frac{3kT}{\zeta b^2}, \tag{37}$$

with b the statistical segment length.

Normalized Rouse mode autocorrelation functions for the three systems are shown in Figs. 12(a) to 12(e) for modes $k=1$ to 5. The first two modes, $k=1$ and $k=2$ are slowed down under the influence of the angular potential (from dashed to dot-dashed lines), in qualitative agreement with the semiflexible chain model of Harnau *et al.*[32] They are slowed down even more in case the uncrossability constraint applies (solid lines). On the other hand, the modes at the smallest scales relax much faster when the chains get some stiffness. Interestingly, these modes relax equally fast with or without uncrossability constraint. So it seems that the uncrossabililty of chains does not affect the relaxation at small scales. However, from Fig. 12(f), which shows the relaxations of the entangled system on a semilogarithmic scale, it is seen that these relaxations are not exponential as predicted by the Rouse model [Eq. (35)]. The reason for this may be that the nonbonded interactions and uncrossability constraints modify the equations of motion and make them highly nonlinear.[21] As a consequence, the Rouse modes can no longer be considered as normal modes of the chains and may no longer relax exponentially.

To quantify the nonexponentiality, the Rouse mode autocorrelation functions were fitted with stretched exponentials,

TABLE II. Amplitude, fit with a stretched exponent, Eq. (38), effective relaxation time and effective relaxation rate as a function of Rouse mode number for the three different systems.

System	k	$\langle \mathbf{X}_k^2\rangle$ (nm^2)	τ_k^* (ps)	β_k	τ_k^{eff} (ps)	W_k^{eff} (ns^{-1})
Unentangled	1	0.725	1920	1.00	1920	1.94
Not stiff	2	0.190	520	0.98	525	1.91
	3	0.094	270	0.96	275	1.82
	4	0.062	185	0.95	195	1.71
	5	0.050	155	0.94	165	1.63
Unentangled	1	1.110	3100	1.00	3100	1.20
Stiff	2	0.227	670	0.96	680	1.47
	3	0.084	250	0.92	270	1.85
	4	0.044	135	0.90	155	2.15
	5	0.031	90	0.87	110	2.44
Entangled	1	0.919	5650	0.94	5515	0.68
Stiff	2	0.192	940	0.80	1065	0.94
	3	0.074	280	0.77	345	1.45
	4	0.040	130	0.77	165	2.02
	5	0.028	80	0.77	110	2.44

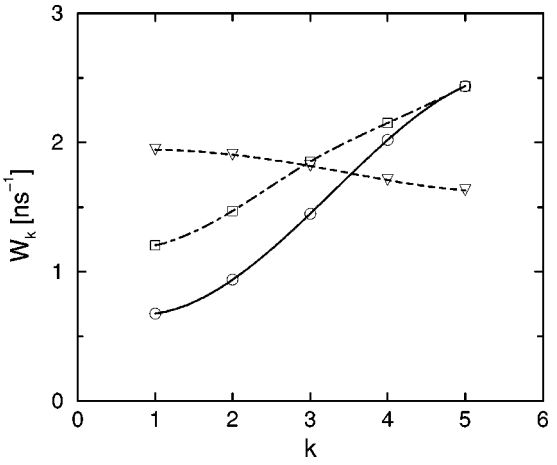

FIG. 13. Effective Rouse relaxation rates as a function of mode number, Eq. (40), for entangled chains (circles), and unentangled chains with (squares) or without (triangles) chain stiffness. The lines are guides to the eye.

$$\langle \mathbf{X}_k(t)\cdot\mathbf{X}_k(0)\rangle/\langle \mathbf{X}_k^2\rangle = \exp[(-t/\tau_k^*)^{\beta_k}], \tag{38}$$

where the relaxation times τ_k^* and stretching parameters β_k depend on mode number k. The fit parameters for the three systems are given in Table II. Two observations can be made: (i) The deviations from exponential behavior ($\beta_k=1$) become larger with increasing mode number, i.e., smaller scales relax increasingly nonexponentially. This is in contradiction with the results of Richter *et al.*,[7] who did not find any hint of stretching in the internal modes, yet in accordance with the results of Shaffer,[21] who placed polymers on a lattice and applied uncrossability constraints. To clear this ambiguity, more experimental evidence of the existence or nonexistence of stretched relaxations will be needed. (ii) Including chain stiffness and uncrossability both make the deviations from exponential behavior become larger, resulting in $\beta_k=0.77$ for modes 3, 4, and 5 in the entangled system. The stretching parameters of Shaffer compared to ours, about 0.75 for the largest mode numbers, although in his case there was less difference between β_k values of crossing and noncrossing polymers. A possible explanation for this smaller difference may be that polymers on a lattice are already more restricted in their motion than polymers in continuum models, so there will be a less pronounced difference between crossing and noncrossing polymers.

In analogy with Shaffer's work, the effective Rouse mode relaxation times were determined as time integrals over the normalized relaxation functions as the macroscopic stress relaxation is governed by these integrals. However, instead of integrating Eq. (38) using the fit parameters, the measured relaxation functions were integrated directly to account for any deviations of the true curves from the fitted curves:

$$\tau_k^{\mathrm{eff}} = \int_0^\infty \langle \mathbf{X}_k(t)\cdot\mathbf{X}_k(0)\rangle/\langle \mathbf{X}_k^2\rangle dt. \tag{39}$$

In analogy to Eq. (36), we define the effective Rouse rate

$$W_k^{\mathrm{eff}} = \left[4\tau_k^{\mathrm{eff}}\sin^2\left(\frac{k\pi}{2N}\right)\right]^{-1}, \tag{40}$$

which, in the case of Rouse chains, is a constant. Effective relaxation times and rates are listed in Table II. As can be seen in Fig. 13, the relaxation rates of the unentangled system without chain stiffness (dashed line) are slightly decreasing with increasing mode number. Because the decrease is relatively small, the relaxation time distribution of this system is essentially Rouse-like. As was already noted, a stiffening of the chain (dot-dashed line) causes slower relaxation of the large scale modes and a faster relaxation of the small scale modes. The uncrossability constraint makes the large scale modes even slower, but leaves the small scale modes unaffected (solid line). We can compare these results with the work of Richter *et al.* who have analyzed dynamic structure factors from neutron spin echo experiments in terms of relevant theoretical approaches.[7] They argued that a stiffening of the chain is essential, but a stiffness correction alone is not enough. Using a realistic value of the stiffness of the chain, their calculations showed that the relaxation times decrease too slowly with increasing mode number to reproduce the experimentally observed dynamic structure factors. These results were questioned by Harnau,[33] but Richter *et al.* argued in response that additional (internal) friction terms may be necessary to explain the experimental results.[34] Our results suggest an alternative additional mechanism. The uncrossability interactions between different (parts of) chains increase the relaxation times of the large scale modes, even for chains which are generally considered not to be entangled.

The crossing over of relaxation rates is often associated with the entanglement length N_e. In Ref. 35, Richter *et al.* argue that the modes with $k \geqslant N/N_e$ are not modified by the entanglement constraints, while modes with $k<N/N_e$ are strongly slowed down. Their Fig. 7 may be compared with our Fig. 13. In our case, the crossing over occurs at $k\approx 3$, i.e., the entanglement length of our model is approximately $6/3=2$ blobs. This corresponds in the microscopic (polyethylene) chain to a length of C_{40}. The values reported in the literature have been going up and down, mainly because the definition of entanglement length was (and still is) unclear. Kremer and Grest found $N_e=35$ for their simulation model,[12] corresponding to C_{97}, Richter *et al.* derived $N_e=136$ monomers, i.e., C_{136}, from their dynamic structure factor measurements,[36] and Carella *et al.* measured $N_e=65$ monomers.[25] Our result is in any case smaller than those from the literature, but this may be due to the fact that our chains are too short to allow for a reasonable estimate of the entanglement length. In a future article, we will vary the chain length and focus more on the entanglement length.

C. Dynamic structure factor

The coherent dynamic structure factor can be measured by means of neutron spin echo spectroscopy. In the experiments conducted by Richter and coworkers, protonated chains were dissolved in a deuterated matrix.[5–7] Because the scattering lengths of protons and deuterons differ, they were able to extract the single chain coherent dynamic structure factor. It can be calculated from

$$S(q,t) = \frac{1}{N_s}\sum_{i=1}^{N_s}\sum_{j=1}^{N_s}\langle \exp\{i\mathbf{q}\cdot[\mathbf{r}_i(t)-\mathbf{r}_j(0)]\}\rangle, \tag{41}$$

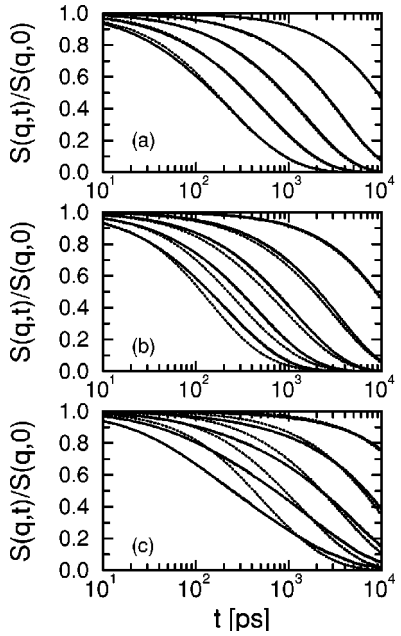

FIG. 14. Single chain dynamic structure factors of entangled chains (c), and unentangled chains with (b) or without (a) chain stiffness (solid lines). In each picture the q values are, from top to bottom: 0.55 nm^{-1}, 1.0 nm^{-1}, 1.4 nm^{-1}, 1.8 nm^{-1}, and 2.2 nm^{-1}. The dotted lines show the fit with the corresponding ($N=6$) Rouse model, using the longest effective relaxation time τ_1^{eff}.

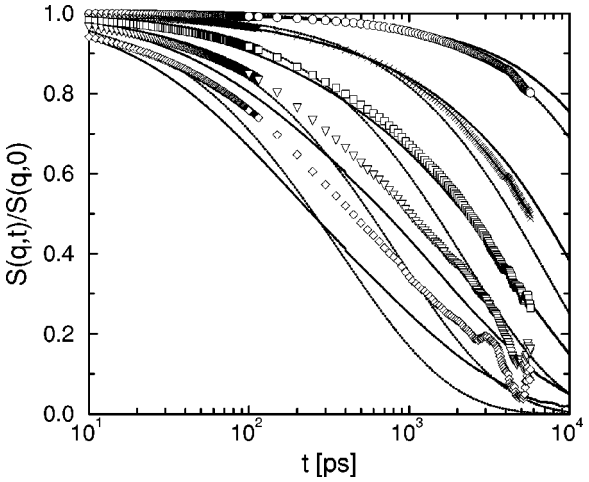

FIG. 15. Single chain dynamic structure factors of entangled mesoscopic chains (solid lines) compared with the results of microscopic molecular dynamics simulations (symbols) and the optimized Rouse fit of Ref. 24 (dotted lines). The q values shown are 0.55 nm^{-1}, 1.0 nm^{-1}, 1.4 nm^{-1}, 1.8 nm^{-1}, and 2.2 nm^{-1}.

where $\mathbf{q}$ is the scattering wave vector and the double summation is over all N_s scattering centers of one chain. Because our chains have been coarse-grained, detailed microscopic information about positions of the hydrogens is lost. However, to a good approximation, the blob positions $\mathbf{R}_i(t)$ can still be used in Eq. (41) to calculate the microscopic dynamic structure factor, provided the wavelength of the scattering wave vector is large compared to the bond length of bonded blobs. As Fig. 2 shows, the maximum bond length is of the order of 2 nm, so q will have to be small compared to 3 nm^{-1}.

The results for five different scattering vectors are shown in Fig. 14 for all three mesoscopic systems (solid lines). Dynamic structure factors were also calculated for corresponding Rouse chains (dotted lines). For each system, the following three Rouse parameters were used: The measured effective first relaxation time τ_1^{eff} (Table II), the measured diffusion coefficient D, and $N=6$ (see the Appendix of Ref. 24 for more Rouse expressions). For the unentangled system without angular potential, Fig. 14(a), the measured curves coincide perfectly with the Rouse curves for all but the largest q vector. This confirms the observation made before that this system can be viewed as essentially Rouse-like. If the chain is made stiffer, Fig. 14(b), the smallest q vector result coincides with the Rouse curve, but all larger q vector results relax slower than the Rouse curves, as was already pointed out by Harnau *et al.*[32,37] If the uncrossability constraint is applied, Fig. 14(c), again the first q vector result coincides with the Rouse curve. All larger q curves not only relax slower, but also do not run parallel to the corresponding Rouse curves. These flattened curves imply a slower relaxation of $S(q,t)$ for large enough times.

In Fig. 15, the results of the entangled mesoscopic model (solid lines) are compared with the results determined from the microscopic simulations described in Ref. 24 (symbols). In this work, an optimized Rouse fit yielded $\tau_1=6.5$ ns, $D=1.15\times10^{-6}$ cm^2/s, and $N=15$. This Rouse result is indicated in Fig. 15 by the dotted lines. As already mentioned, the present works friction ξ was determined by matching the diffusion coefficient of the mesoscopic model with that of the microscopic model, but because of inaccuracy of the interpolation, a slightly smaller diffusion coefficient was obtained. As a result, all small q dynamic structure factor results are slightly above the microscopic results. Despite this inaccuracy, it is clear that the entangled mesoscopic model yields results which are far more better than the Rouse predictions. The results for q equal to 0.55, 1.0, and 1.4 nm^{-1} are in perfect agreement with the microscopic chain. The results for both of the large q values, 1.8 and 2.2 nm^{-1}, suffer from the lack of microscopic detail. In all cases, the slopes are in agreement with the microscopic results, from which we conclude that our model captures the physics much better than the Rouse model.

D. Shear relaxation modulus and viscosity

In a nonperiodic system, the stress tensor in the presence of entanglements may be given by

$$\boldsymbol{\sigma}=\frac{1}{V}\left[\sum_{i=1}^{n} M\mathbf{V}_i\mathbf{V}_i+\mathbf{R}_i\mathbf{F}_i\right]+\frac{1}{V}\left[\sum_{k=1}^{p}\mathbf{X}_k\mathbf{G}_k\right]. \tag{42}$$

The first bracketed term is the standard expression for the stress tensor in a nonperiodic system of n particles without entanglements: $\mathbf{V}_i$ is the velocity, and $\mathbf{F}_i$ is the force on particle i. The second bracketed term contains the sum of all products of entanglement positions $\mathbf{X}_k$ and corresponding forces $\mathbf{G}_k$. This term may be added because the total force on each entanglement is zero. In the presence of entanglements, the attractive forces appear as pair interactions between nearest neighbors along the chains, be they blobs or

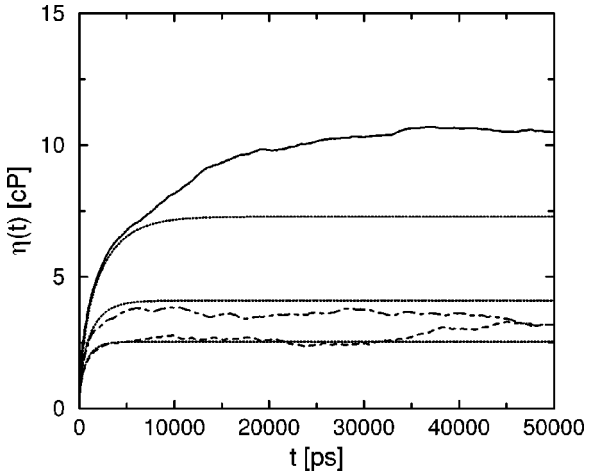

FIG. 16. Integral of the zero shear relaxation modulus up to time t, Eq. (44), of entangled chains (solid), and unentangled chains with (dot-dashed) or without chain stiffness (dashed). The dotted lines show the Rouse integrals determined by using the longest effective relaxation time τ_1^{eff}.

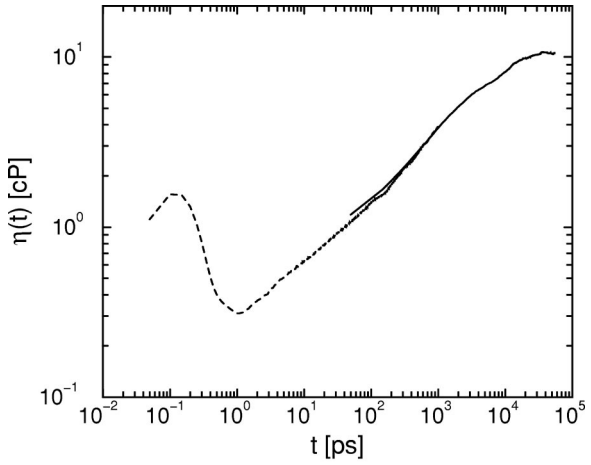

FIG. 17. Integral of the zero shear relaxation modulus up to time t of the entangled mesoscopic model (solid) and from microscopic molecular dynamics simulations (dashed) on a double-logarithmic scale.

entanglements [see Eq. (17) and the discussion following this equation]. Since these pair interactions obey Newtons third law, we may apply the usual transformation to a periodic system in order to calculate the contribution of the attractive forces to the stress tensor. The remaining contributions to the stress tensor, due to the angular, nonbonded, and repulsive interactions between bonded blobs, are related to the blob positions only, and can be calculated in the usual way.

The zero shear relaxation modulus is related to the symmetrized traceless part $\mathbf{P}$ of the stress tensor $\boldsymbol{\sigma}$ by[38]

$$G(t)=\frac{V}{10kT}\langle \mathbf{P}(t):\mathbf{P}(0)\rangle. \tag{43}$$

The double contraction means that, in practice, we can average over five independent contributions: P_{xy}, P_{xz}, P_{yz}, $1/2(P_{xx}-P_{yy})$, and $1/2(P_{yy}-P_{zz})$. Figure 16 shows the integrals of the zero shear relaxation modulus up to time t,

$$\eta(t)=\int_0^t G(t)dt, \tag{44}$$

for the three mesoscopic models, together with the Rouse predicted integrals using the effective first Rouse times τ_1^{eff} (dotted lines). The unentangled system without chain stiffness (dashed line) follows the Rouse curve quite well, so the viscosity equals that of the corresponding Rouse chain, i.e., 2.5 cP. With chain stiffness (dot-dashed line), the integral systematically lies beneath the Rouse result. This can be explained by the fact that the viscosity of a Rouse melt is proportional to the sum of all relaxation times (see the Appendix of Ref. 24). The Rouse curve in Fig. 16 was calculated using a relaxation time spectrum obtained from the first, largest scale relaxation time, but, as it was shown before, the small scale modes actually have shorter relaxation times. Still, the increased chain stiffness has increased the viscosity to approximately 3.6 cP. The result of the entangled system is quite remarkable (solid line). Initially, it follows the Rouse prediction up to $t=5$ ns, but then continues to increase where the Rouse prediction is already converged. The following mechanism may explain this result: Initially the stress due to intrachain interactions predominates the stress due to interchain interactions and the relaxation is rather Rouse-like. However, after the intrachain stress has relaxed, the interchain stress still remains. This interchain stress relaxes slower than the slowest intrachain relaxation, i.e., slower than τ_1. This interchain stress will eventually bring about the plateau modulus for longer chains.

Figure 17 shows the integrals of both the microscopic and entangled mesoscopic systems on a double-logarithmic scale. Here the strength of the coarse-grained simulation, combined with the entanglement algorithm is apparent: After a comparable run time of a few months, the microscopic simulations reached correlation times up to 1 ns, while the coarse-grained simulations reached up to 50 ns (notice that the coarse-grained system contained ten times as many chains). At medium long times, the mesoscopic results are nicely following the microscopic results, so we have confidence that the coarse grained-model can predict the viscosity. From the asymptotic value of the integral, we estimate the viscosity of a $C_{120}H_{242}$ chain at 450 K to be $\eta\approx 10.5$ cP. This is in good agreement with (interpolated) experimental results of Pearson *et al.*, who found $\eta_{\text{exp}}\approx 13.5$ cP.[1]

VI. CONCLUSIONS

We have investigated the influence of uncrossability constraints on the dynamics of coarse-grained polymer melts. In the first part of this work, we have described how such a constraint may be implemented in a continuum simulation model. We next have applied our method to a $C_{120}H_{242}$ melt, represented by chains composed of six blobs. In order to investigate the importance of various aspects of our model, we have simulated two other systems, both without the uncrossability constraint: One with and one without chain stiffness. We have found that the uncrossability constraint is essential to reproduce microscopic dynamic correlation functions. We summarize our findings in the following points:

1. Neither one of the unentangled systems shows a subdif-

fusive exponent in the mean square displacement of the center of mass of the chain; the entangled system does. The subdiffusive exponent must be caused by uncrossability interactions with the surrounding chains.

2. The Rouse mode autocorrelation functions of the unentangled system without chain stiffness are rather Rouse-like. The other two systems clearly display a stretching of the exponential decay, which becomes most pronounced for the smallest scales in the entangled system ($\beta = 0.77$). For stiff chains, the effective relaxation rates of small scale modes increase and those of large scale modes decrease, in agreement with semiflexible chain models. The uncrossability constraint causes an even slower relaxation of the large scale modes.

3. The single chain dynamic structure factor of the unentangled system without chain stiffness displays a Rouse-like decay. The incorporation of chain stiffness yields slower decaying curves, but this is not enough to reproduce the microscopic data. For q values smaller than 1.8 nm^{-1}, the results of a microscopic simulation are well-reproduced by the entangled system. Results for larger q values cannot be reproduced because the coarse-grained simulations suffer from a lack of microscopic detail.

4. The shear relaxation modulus of the unentangled system without chain stiffness behaves Rouse-like. The inclusion of chain stiffness has some effect because the relaxation spectrum is modified. In the entangled system, an initial Rouse-like relaxation is observed. After $t = 5$ ns the chain relaxes more slowly than a Rouse chain. This must be due to a very slow interchain stress relaxation caused by the uncrossability of chains. This interchain stress is dominated by the intrachain stress relaxation at shorter times. The viscosity found for this system ($\eta \approx 10.5$ cP) is close to experimental findings.

In a future article, we will increase the chain length N to investigate the scaling of dynamic properties. We will pay attention to the entanglement length, entanglement distributions, and correlation functions. We will also investigate how a plateau in the shear relaxation modulus develops with increasing N.

[1] D. S. Pearson, G. Ver Strate, E. von Meerwall, and F. C. Schilling, Macromolecules **20**, 1133 (1987).
[2] C. B. Gell, W. W. Graessley, and L. J. Fetters, J. Polym. Sci., Part B: Polym. Phys. **35**, 1933 (1997).
[3] L. J. Fetters, D. J. Lohse, D. Richter, T. A. Witten, and A. Zirkel, Macromolecules **27**, 4639 (1994).
[4] L. J. Fetters, D. J. Lohse, and W. W. Graessley, J. Polym. Sci., Part B: Polym. Phys. **37**, 1023 (1999).
[5] W. Paul, G. D. Smith, D. Y. Yoon, B. Farago, S. Rathgeber, A. Zirkel, L. Willner, and D. Richter, Phys. Rev. Lett. **80**, 2346 (1998).
[6] P. Schleger, B. Farago, C. Lartigue, A. Kollmar, and D. Richter, Phys. Rev. Lett. **81**, 124 (1998).
[7] D. Richter, M. Monkenbusch, J. Allgeier, A. Arbe, J. Colmenero, B. Farago, Y. Cheol Bae, and R. Faust, J. Chem. Phys. **111**, 6107 (1999).
[8] P. E. Rouse, J. Chem. Phys. **21**, 1273 (1953).
[9] M. Doi and S. F. Edwards, *The Theory of Polymer Dynamics* (Clarendon, Oxford, 1986).
[10] M. Pütz, K. Kremer, and G. S. Grest, Europhys. Lett. **49**, 735 (2000).
[11] T. P. Lodge, N. A. Rotstein, and S. Prager, Adv. Chem. Phys. **79**, 1 (1990).
[12] K. Kremer and G. S. Grest, J. Chem. Phys. **92**, 5057 (1990).
[13] S. W. Smith, C. K. Hall, and B. D. Freeman, J. Chem. Phys. **104**, 5616 (1996).
[14] K. M. Zimmer, A. Linke, and D. W. Heermann, Macromol. Theory Simul. **5**, 1065 (1996).
[15] G. Schöppe and D. W. Heermann, Phys. Rev. E **59**, 636 (1999).
[16] W. Tschöp, K. Kremer, T. Bürger, and O. Hahn, Acta Polym. **49**, 61 (1998).
[17] J. Baschnagel *et al.*, Adv. Polym. Sci. **152**, 41 (2000).
[18] R. L. C. Akkermans and W. J. Briels, J. Chem. Phys. **113**, 6409 (2000).
[19] In the extreme case, a polymer chain has been represented as a single soft ellipsoidal particle. In this case, of course, all entanglement effects are neglected which results in unrealistic dynamics. M. Murat and K. Kremer, J. Chem. Phys. **108**, 4340 (1998).
[20] J. S. Shaffer, J. Chem. Phys. **101**, 4205 (1994).
[21] J. S. Shaffer, J. Chem. Phys. **103**, 761 (1995).
[22] Y. Termonia, Macromolecules **29**, 2025 (1996).
[23] J. T. Padding and W. J. Briels, TWENTANGLEMENT User's manual (Twente University, 2000).
[24] J. T. Padding and W. J. Briels, J. Chem. Phys. **114**, 8685 (2001).
[25] J. M. Carella, W. W. Graessley, and L. J. Fetters, Macromolecules **17**, 2775 (1984).
[26] A third possibility is that the length of either vector becomes zero. In this rare case, impreciseness of the minimization step may lead to false (dis)entanglements. Therefore, if the distance between two connected objects is smaller than ϵ (introduced in Sec. III D) it is not allowed to (dis)entangle.
[27] Only in an extremely rare case will two line segments simultaneously cross and alter relative orientation during one time step. In that case, V_{ij} will not alter sign. We are disregarding entanglements and disentanglements of this kind.
[28] M. P. Allen, Mol. Phys. **40**, 1073 (1980); **47**, 599 (1982).
[29] W. F. van Gunsteren and H. J. C. Berendsen, Mol. Phys. **45**, 637 (1982).
[30] W. Paul, G. D. Smith, and D. Y. Yoon, Macromolecules **30**, 7772 (1997).
[31] W. J. Briels, *Theory of Polymer Dynamics*, Lecture Notes, Uppsala (1994). The full text can be downloaded from http://www.tn.utwente.nl/cdr/PolymeerDictaat/
[32] L. Harnau, R. G. Winkler, and P. Reineker, Europhys. Lett. **45**, 488 (1999).
[33] L. Harnau, J. Chem. Phys. **113**, 11396 (2000).
[34] D. Richter, M. Monkenbusch, W. Pykhout-Hintzen, A. Arbe, and J. Colmenero, J. Chem. Phys. **113**, 11398 (2000).
[35] D. Richter, L. Willner, A. Zirkel, B. Farago, L. J. Fetters, and J. S. Huang, Macromolecules **27**, 7437 (1994).
[36] D. Richter, R. Butera, L. J. Fetters, J. S. Huang, B. Farago, and B. Ewen, Macromolecules **25**, 6156 (1992).
[37] L. Harnau, R. G. Winkler, and P. Reineker, Phys. Rev. Lett. **82**, 2408 (1999).
[38] P. J. Daivis and D. J. Evans, J. Chem. Phys. **100**, 541 (1994).